SLAC – PUB – 3846
December 1985
(T/E)

Single Photon Searches at PEP*

R. HOLLEBEEK

Stanford Linear Accelerator Center
Stanford University, Stanford, California, 94305

ABSTRACT

The MAC and ASP searches for events with a single photon and no other observed particles are reviewed. New results on the number of neutrino generations and limits on selectron, photino, squark and gluino masses from the ASP experiment are presented.

Presented at the SLAC Summer Institute on Particle Physics
Stanford, California, July 29 – August 9, 1985

* Work supported by the Department of Energy, contract *DE – AC03 – 76SF00515.*

CONF-850108--7

DE-AC03-76SF01588-1

Introduction

During the past year, two experiments have been carried out at PEP to search for events with a photon and large missing transverse momentum . These event searches are particularly sensitive to contributions from supersymmetric photino production but can also be used to search for additional neutrino generations, supersymmetric weak charged currents or the production of any other neutral particle whose interactions in matter are of the order of the weak interaction. The MAC collaboration began modifications of their apparatus during the summer of 1983 to be able to detect photon events with no other observed charged or neutral particles. At the same time, a new experiment, ASP, was approved for installation at the PEP ring to do a high sensitivity search for such events.

Single Photon Sources

In the standard model of weak and electromagnetic interactions, events with a single photon and no other observed particles will be produced by radiative corrections to the production of neutrino pairs.

$$\sigma(e^+e^- \to \gamma\nu\bar{\nu}) \sim \alpha G_F^2 s \left(1 + \frac{N_\nu}{4}\right) \quad .$$

Since this cross-section is of order αG_F^2 , one might think that it is too small to measure, but in fact, the total cross-section for reasonable assumptions about the photon acceptance is a few times 10^{-2} pb at PEP and is therefore detectable. This process receives contributions from the weak neutral currents (Fig. 1(a)) proportional to the number of neutrino generations and from the production of electron neutrinos through the charged weak currents (Fig. 1(b)). Because of the sensitivity of the cross-section to the presence of all generations of light neutrinos, this process has been suggested[1] as a means of counting the number of different types of neutrinos and hence placing limits on the number of lepton generations. Unlike many other methods of counting generations, this technique

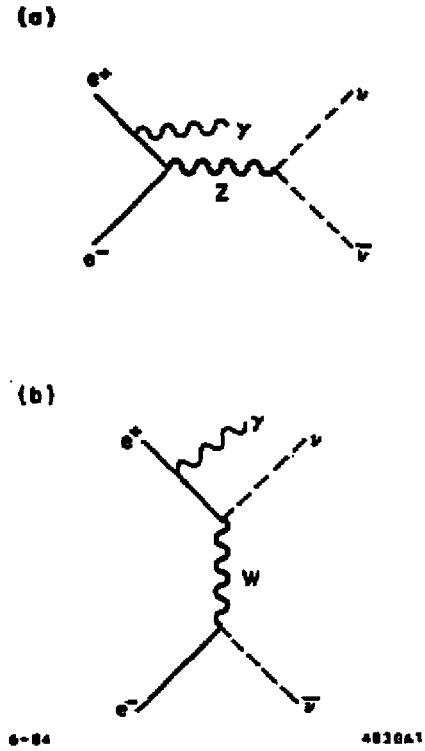

Fig. 1. Single photon contributions from the weak (a) neutral and (b) charged currents.

has the advantage of being insensitive to the masses of the associated charged leptons which are observed to increase rapidly with generation number in our present examples.

In addition to the standard model sources of single photon events, many models of new physics contain particles which can be stable and which interact in matter with a cross-section which is of the order of magnitude of the weak cross-section. If the cross-section for production of events containing only these particles is known, then the single photon rate can be calculated from the radiative corrections to that cross-section. For example, if σ_0 is the cross-section for the production of such a state, then the single photon rate is given by

$$\frac{d^2\sigma}{dx_\gamma d\cos\theta_\gamma} = \frac{2\alpha}{\pi}\,\frac{1}{x_\gamma}\,\frac{1}{\sin^2\theta_\gamma}\,\sigma_0(s')$$

where $s' = s(1 - x_\gamma)$ is the reduced center of mass energy squared.

Supersymmetry is an example of a model of new physics in which there are many possibilities for events which contain only weakly interacting neutral particles. Final states which might behave this way are photino pairs, zino pairs, or sneutrino pairs. Because of a conserved quantum number (R parity), the lightest supersymmetric particle would be stable, and cosmological arguments indicate that it is probably neutral.[2,3] Possible candidates for the lightest neutral sparticle are the photino ($\tilde{\gamma}$), the neutral shiggs ($\tilde{H}$) and the gravitino ($\tilde{G}$). Since these are all fermions, they may be protected by chiral symmetry from attaining a large mass due to supersymmetry breaking. Of course, the sneutrino ($\tilde{\nu}$), although it is a boson may also be the lightest neutral supersymmetric particle.

As pointed out by Fayet and others,[4,5] a search for single photon states is a particularly sensitive way of testing supersymmetry if the photino is light. The radiative correction to photino pair production is

$$\sigma(e^+e^- \to \gamma\tilde{\gamma}\tilde{\gamma}) \sim \alpha^3\frac{s}{m_{\tilde{e}}^4}$$

where $m_{\tilde{e}}$ is the mass of the spin zero partner of the electron (selectron). Since

the coupling constant of the supersymmetric particles is still α, the calculation proceeds as in QED except for spin factors and masses (see Fig. 2). If we compare the supersymmetric source of single photons to the cross-section for single photon events in the standard model using

$$\alpha G_F^2 \sim \frac{\alpha g_{WS}^4}{m_W^4} \sim \frac{\alpha^3}{\sin^4(\theta_{WS}) m_W^4} \quad ,$$

we can see that it is possible to have sensitivity to selectron masses of order m_W. If the selectron is sufficiently heavy, the interaction cross-section of photinos in matter will be small and they will not be detected. This photino interaction cross-section is determined by[4]

$$\sigma(e\tilde{\gamma} \to e\tilde{\gamma}) = \frac{8\pi}{3} \alpha^2 \frac{s}{m_{\tilde{e}}^4}$$

so that

$$\frac{\sigma_{\tilde{\gamma}}}{\sigma_\nu} \sim 50 \left(\frac{40 \text{ GeV}}{m_{\tilde{e}}^4}\right)$$

and thus if the selectron mass is a few tens of GeV, the photinos will escape detection.

Because the detected final state is the same and because the Feynman diagrams of Fig. 1(b) and Fig. 2 are similar, the two processes which have been considered so far have very similar differential cross-sections. Except for the addition of small corrections for photons radiated from the W or selectron, the cross-sections in the local limit ($s \ll m^2$) for photons with $x = 2E/\sqrt{s}$ are

$$\frac{d^2\sigma}{dx\,dy} = K \frac{1}{x} \frac{1}{1-y^2} s(1-x) \left[\left(1 - \frac{x}{2}\right)^2 + \frac{x}{4} y^2\right]$$

where

$$K_{\gamma\nu\bar{\nu}} = \frac{G_F^2 \alpha}{6\pi^3} \left[N_\nu \left(g_V^2 + g_A^2\right) + 2\left(g_V + g_A + 1\right)\right] \quad ,$$

$$K_{\gamma\tilde{\gamma}\tilde{\gamma}} = \frac{4\alpha^3}{3m_{\tilde{e}}^4}$$

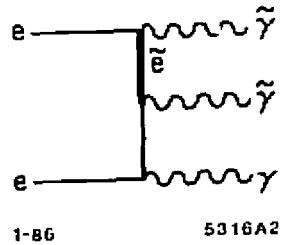

Fig. 2. Feynman diagram for $e^+e^- \to \gamma\tilde{\gamma}\tilde{\gamma}$.

and $y = \cos\theta_\gamma$. A limit on the single photon cross-section probes the sum of the neutrino pair and the supersymmetric sources, so one might think of the generation counting process as a "background" to the search for new physics. In this case, for $m_{\tilde{\nu}} > \sqrt{2}m_W$ the weak cross-section for $\gamma\nu\bar{\nu}$ dominates and the only way to separate the two is a careful study of the $\sqrt{s}$ dependence since the weak cross-section has a resonance and the supersymmetric cross-section does not. The possibility of new physics is also a background for the generation counting experiment. Because of this, we will not be able to interpret the results of SLC and LEP studies of the Z width without using the lower energy (PEP) data.

If the sneutrino is the lightest supersymmetric particle,[6] single photon events will be produced by the standard weak neutral current and the supersymmetric charged currents (see Fig. 3). In the neutral current diagram, the size of the cross-section is determined by the number of light sneutrinos. Due to spin factors, each sneutrino generation adds to the cross-section an amount equivalent to half that of a neutrino generation. For the charged currents, the cross-section is determined by the masses of the charged weak fermions $\tilde{W}^{\pm}$ which may be different and by the mixing angles[7] between them and the higgsinos. It is still possible, however, to place a model independent limit on the cross-section for such processes since the photon spectrum is insensitive to these parameters. The interpretation of the cross-section in terms of masses will depend on the mixing angle assumptions.

Supersymmetric theories postulate a new symmetry of nature between bosons and fermions and hence predict many new particles. Within this theory, every particle has a supersymmetric partner with opposite spin statistics and since no pair of particles in our current particle table is known to be a particle-sparticle pair, there are as many new particles as old ones! Clearly the theoretical community must be highly motivated to propose such an idea . In order to understand this, we should look carefully at the standard model of weak and electromagnetic interactions. Despite the obvious successes of the Weinberg-Salam-Glashow model, there is one outstanding problem related to the Higgs mass. The Higgs boson is crucial within the theory for generating the masses of the weak bosons,

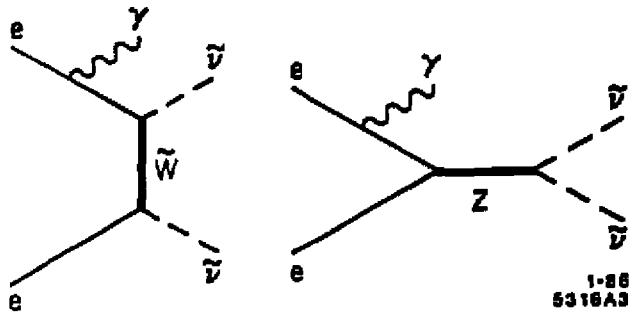

Fig. 3. Feynman diagrams for $e^+e^- \to \tilde{\nu}\tilde{\nu}\gamma$.

yet many particle searches have failed to locate such a particle leading to speculations that it's mass may be large. Theoretically, the mass is very large since higher order corrections cause it to be ultraviolet divergent. There are two possible solutions to the problem: give the Higgs internal structure so that large corrections to it's mass are cut off by a form factor, or introduce new interactions which cancel the higher order terms. Supersymmetry is an example of the latter approach because for every boson loop contribution to the Higgs mass, there is an opposite sign contribution from a partner fermion loop. This cancellation would be complete if the masses of the fermions and bosons were degenerate, but in general the correction to the Higgs mass has the form[8]

$$\delta_{M_H^2} \sim \frac{g^2}{16\pi^2}\,(m_B^2 - m_F^2) \quad .$$

Note that if the superpartners are too heavy relative to normal matter, supersymmetry can no longer be looked on as a solution to the higgs mass problem.

While supersymmetry is of great interest at the moment because of the way in which it solves divergence problems in the standard model and within quantum gravity, we may in the future find other means of solving these problems. In this case, the single photon cross-section will remain a powerful test of any model of new physics which contains particles which interact weakly in matter.

Single Photon Detection

Because the radiative cross-section varies like

$$\frac{1}{x_\gamma}\,\frac{1}{\sin^2\theta_\gamma} \quad ,$$

it is important to detect photons at as small an energy and angle relative to the beam energy and angle as possible. In the energy dependence, the integrated rate will vary as $\ln x_{min}$ so that the difference between a 2 and a .25 GeV threshold

at PEP will be a factor of two in the observable rate. Similar factors can be obtained from the $\sin\theta$ dependence. This is illustrated in Fig. 4 which shows monte carlo data folded with efficiency for events within the ASP detector as a function of the energy and angle of the detected photon. Note the rapid increase in the cross section for low energy and angles.

In addition to having as large an acceptance as possible, it is also necessary to show that the detected events are accompanied only by neutrinos or other weakly interacting particles. This is particularly important because of the presence of radiative corrections to QED production of electron, photon, muon, and tau pairs. The cross-section for $ee \rightarrow \gamma ee$ is the largest background and requires a rejection of $\sim 10^{-4}$ to reach a sensitivity to neutrino pair production. Fortunately this level of rejection can be achieved by using the kinematics of the three-body final state. As shown in Fig. 5, the transverse momentum of the detected photon relative to the beam line must be balanced by the electron pair. Thus for a detected photon with transverse momentum p_t^γ, at least one of the other particles will be at an angle larger than

$$\sin\theta_{recoil}^{min} \approx \frac{E_t^\gamma}{2E_{beam} - E_\gamma} \quad .$$

As an example, for a photon with 1 GeV/c of transverse momentum, detection of additional particles must extend to a veto angle less than 36 mrad at PEP. In practice, the veto angle for QED processes can be almost a factor of two larger because for soft photons the QED matrix elements are dominated by the case where the photon tends to be balanced by only one of the other particles. This results in a decrease of the cross section between the above recoil angle and

$$\theta_{recoil}^{min} \sim \frac{E_t^\gamma}{E_{beam}} \quad .$$

For a 1 GeV/c transverse momentum cut , the required veto angle now becomes roughly 69 mrad. Figure 6 shows the results of a QED Monte Carlo calculation of the $ee\gamma$ cross section as a function of the $\cos\theta$ of the electron scattered through

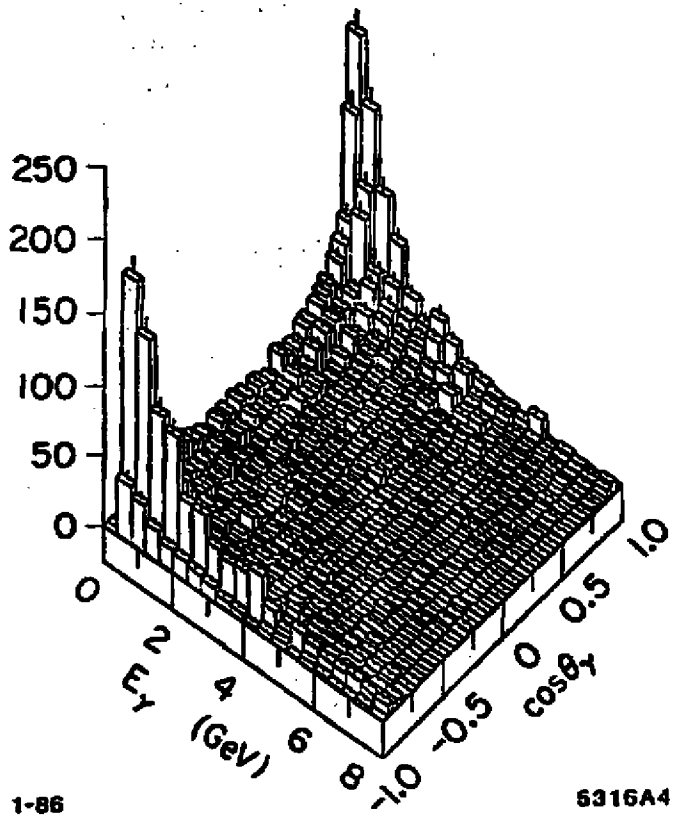

Fig. 4. Monte carlo data in the ASP acceptance $\sigma(ee \to \gamma\nu\bar{\nu})$.

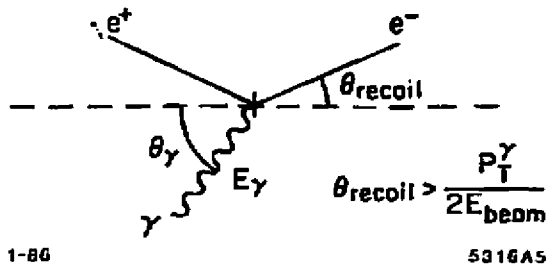

Fig. 5. Kinematics used to eliminate QED backgrounds.

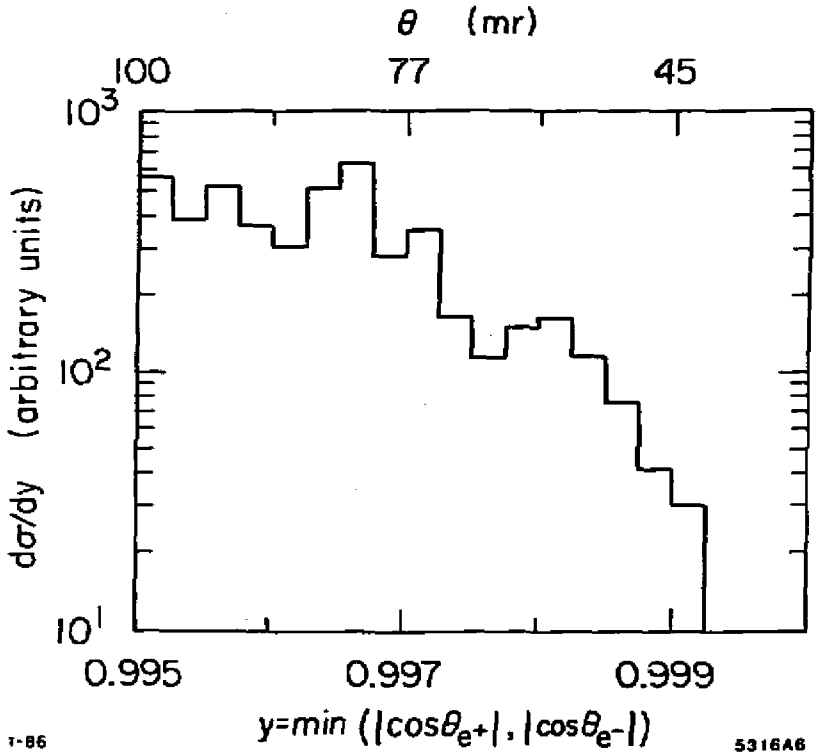

Fig. 6. QED Monte Carlo calculation of $\sigma(ee\gamma)$ versus $\cos\theta_e$.

the maximum θ when the detected photon has at least 1 GeV/c of transverse momentum.

Because of the large number of events which must be rejected, it is important that there be *no regions* of the detector through which charged particles or photons can pass undetected. These are usually referred to as "cracks" and can occur for example in the gaps between azimuthal segmentations of a calorimeter or in the transition region between calorimeters at large and small values of theta. Special care must be taken to either cover all such areas with detection equipment or to have a design which has no cracks. Covering the cracks can sometimes be difficult since the background from $\gamma\gamma\gamma$ events requires that the detector be thick enough so the non-conversion probability of photons is small.

The MAC Experiment

The MAC detector[9] is shown in Fig. 7. The shower counter (SC) used to detect photon candidates consists of 32 lead plates interspersed with proportional wire chambers for a total thickness of 14 radiation lengths. The proportional wires are parallel to the beam axis and are contained in 1 cm $\times$ 2 cm aluminum extrusions. Positions along the wire are obtained by charge division readout with 4 cm resolution. Groups of wires are combined together such that the detector has three segments in depth and an azimuthal segmentation of 1.9°. Photon candidates are required to be more than 40° from the beam axis so that the shower is contained in the SC. The endcap hadronic calorimeter (EC) extends to roughly 10° and is used as a veto. It consists of 28 1-inch-thick steel plates each followed by planar proportional chambers constructed in 30° wedges. There is a gap of about 10 cm between the wedges. Segmentation in the EC is 5° in both θ and ϕ with four layers in depth. Events with charged particles can be vetoed using the central drift chamber which has 10 layers of drift cells with at least 5 layers for particles at more than 17° from the beam axis.

Two samples of data have been reported.[10] In the first sample of 36 pb^{-1},

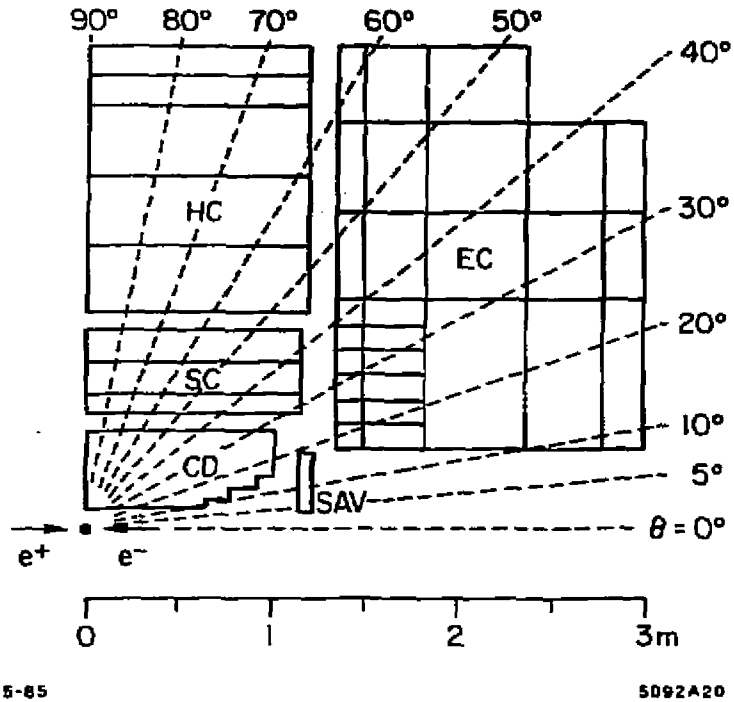

Fig. 7. The MAC Detector: central drift chamber (CD), shower counter (SC), central and endcap hadron calorimeters (HC, EC), and small angle veto (SAV).

a small angle veto system was not installed, hence the minimum veto angle of $\sim 10°$ required a *missing transverse momentum* of greater than 4.5 GeV for a complete veto of the QED backgrounds. When a small angle veto (SAV) system was installed, it reduced the veto angle to 5° which extends the search region to $E_{t\gamma} > 3$ GeV. The SAV (see Fig. 8) is constructed from lead and proportional chambers and is 8.5 radiation lengths thick. A total of 80 pb^{-1} was collected with this configuration.

Backgrounds to the search can occur from cosmic rays, electronic noise, and from beam related backgrounds such as scattering from upstream masks, beam-halo, and beam-gas interactions. The hits in the SC from cosmic rays or bursts of electronic noise have wider azimuthal angular spreads on average than photon showers, so cuts are placed on the width of each shower candidate. The hits are fitted with a straight line to determine an origin for the event (z_0) along the beam axis and a distance of closest approach r_{min} to the beam axis in the plane perpendicular to the beam. The resolution in these quantities is 12 cm and 3.3 cm respectively. Showers are required to have $|z_0| < 30$ cm and $r_{min} < 15$ cm.

The trigger for the search requires > 2.0 GeV in one of the SC sextants plus at least two of three layers in depth with > 0.3 GeV in the 10° veto sample. The 5° veto sample requires 1.5 GeV in the SC and two layers with more than 0.25 GeV. Figure 9 shows the trigger efficiency measured using a sample of single electron events which are tagged with the forward detector. When combined with the analysis efficiency and plotted as a function of E_t (Fig. 10) the overall efficiency is found to rise with increasing $E_{t\gamma}$ from $(67 \pm 5\%)$ at 3 GeV to $(73 \pm 5\%)$ at 10 GeV. When folded with the radiative photon spectrum, this yields an overall efficiency of 71% for the first data sample, and 69% for the second.

The distribution of events seen as a function of the missing transverse momentum is shown in Fig. 11 for the data samples with 4.5 GeV and 3.0 GeV veto capabilities. The event levels below the search regions are roughly compatible with the background estimates shown, and one event is observed in the search

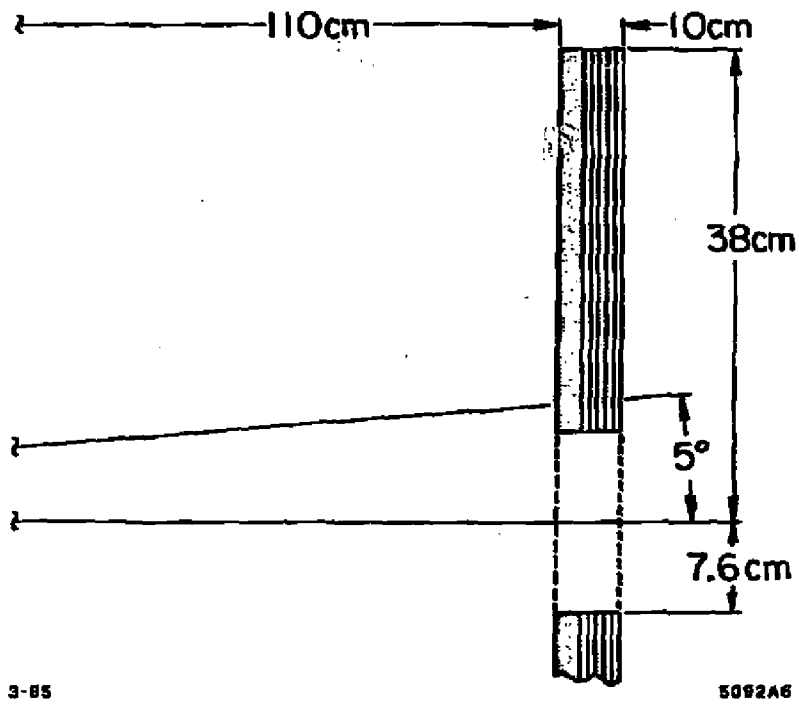

Fig. 8. Construction detail – MAC small angle veto.

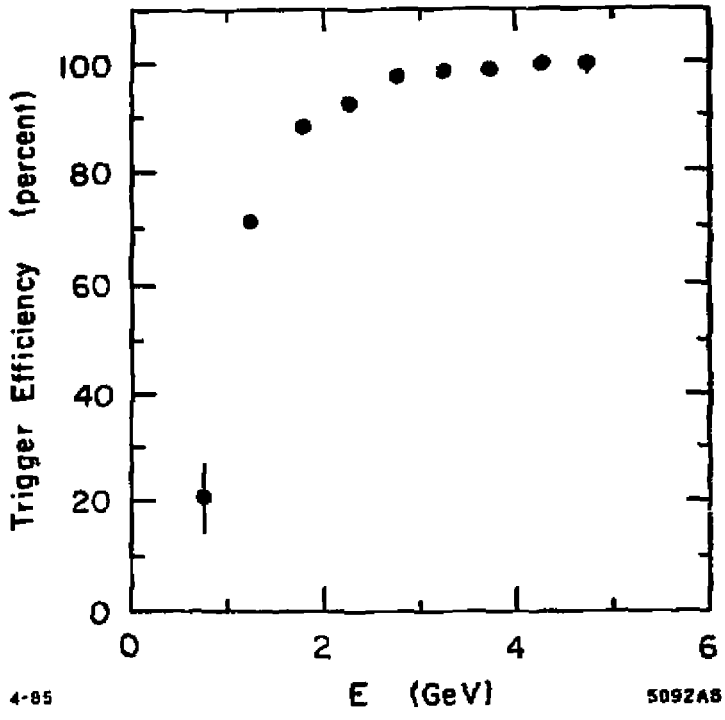

Fig. 9. Trigger efficiency versus energy – MAC.

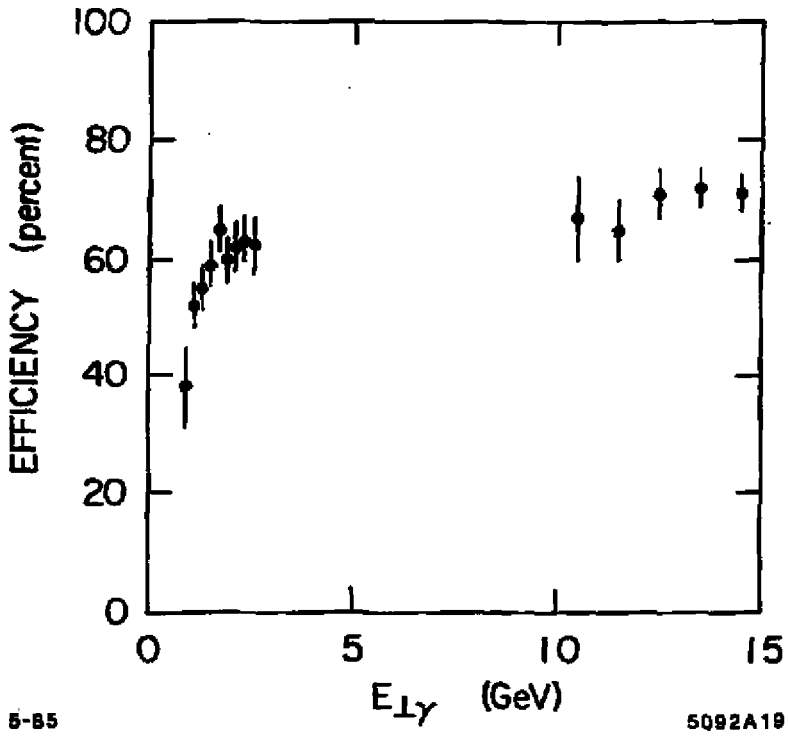

Fig. 10. MAC – Trigger and analysis efficiency versus photon transverse momentum.

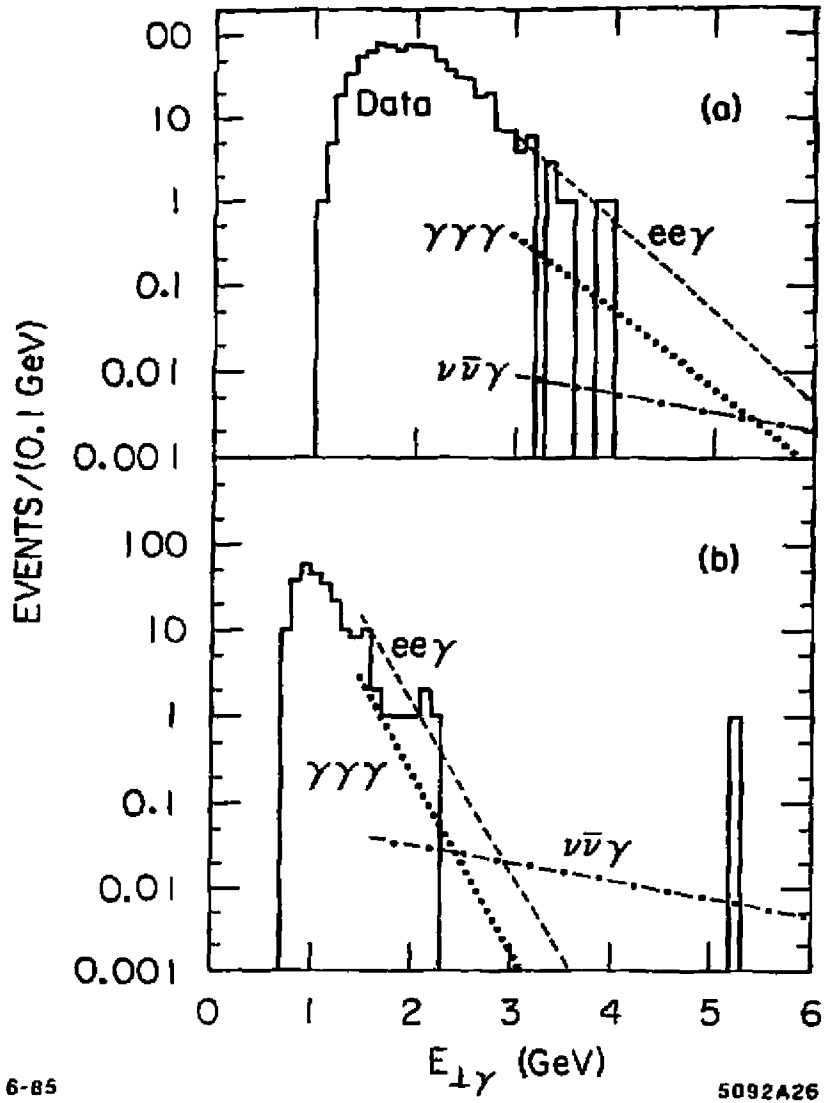

Fig. 11. MAC – Single photon events seen as a function of E_t in the sample with (a) $\theta_{veto} = 10°$ and (b) $\theta_{veto} = 5°$.

region of the second sample. The estimated background contribution from all sources is less than 0.3 events, with a signal of 0.5 event expected from $\gamma\nu\bar{D}$ production for 3 generations.

MAC Limits

The one event observed in the sample corresponds to a 90% confidence limit of 3.9 events within the luminosity and efficiency weighted average of the two samples previously discussed. This corresponds to a cross-section limit of $<$ 0.057 nb. When interpreted as a limit on neutrino generations, it requires $N_\nu <$ 41. To interpret the result in terms of supersymmetry, a subtraction is made for the $\nu\bar{D}\gamma$ cross-section corresponding to the expected value for three generations of neutrinos, and the excess is used to obtain the limits for $\tilde{e}$ and $\tilde{\gamma}$ masses shown in Fig. 12.

MAC – 1985

During the summer of 1984, a 4 atm. pressurized vertex chamber of the straw type was installed in the central region of the MAC detector. Unfortunately, vertex detection and single photon detection have somewhat conflicting requirements. The vertex chamber introduces considerable inactive material in the small angle region due to its endplates, pressure plate and electronics. It also requires masks to shield it from synchrotron radiation. In the MAC detector, Hevimet shielding and tantalum masks were installed which would eliminate the ability of the SAV system to veto below 7.3°. BGO calorimeters were installed immediately in front of these masks to allow the detector to continue to veto at small angles. There are two problems with this approach. First, since the region of the beamline which is unmasked is comparable to the resolution along the beam axis for single photon candidates, it is difficult to determine the contamination in the signal region from events which come from beam-halo or beam-gas interactions. (This is normally done by looking at the signal from regions outside

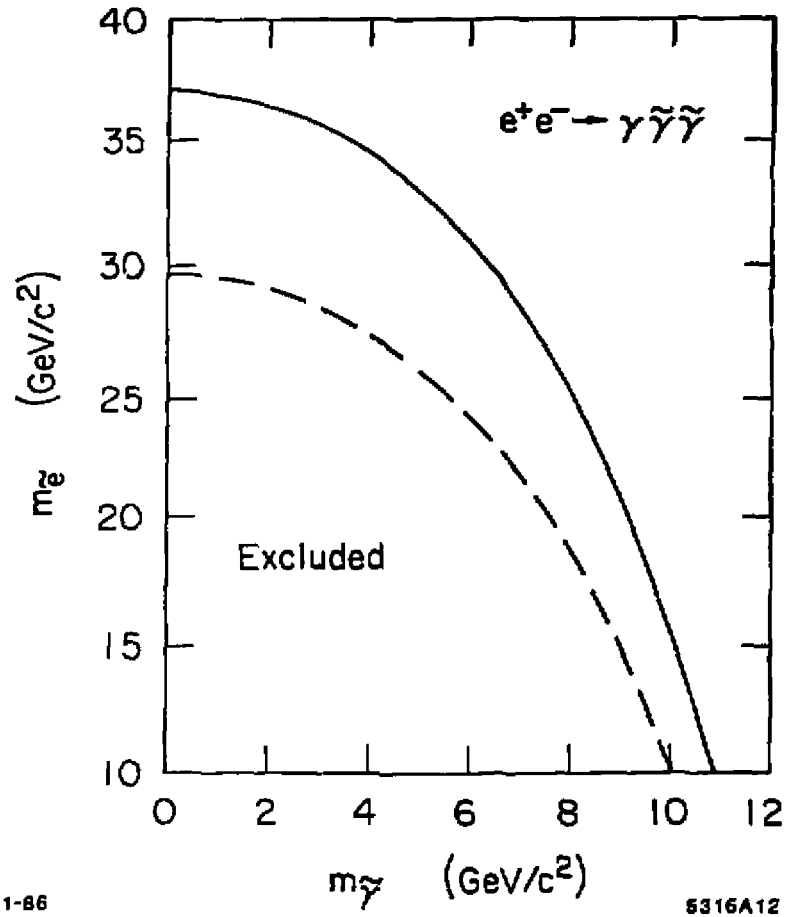

Fig. 12. MAC – Excluded region in $m_{\tilde{e}}$ and $m_{\tilde{\gamma}}$ for 90% confidence.

of the central region.) Second, the mask itself can become a significant source both of events, and of backgrounds or occupancy in the BGO veto. Data from the 1985 run is still being processed, however with the presence of the ASP detector and the problems mentioned above, the emphasis has shifted from single photon physics to vertex physics.

ASP – A Detector Optimized for Single Photons

The ASP detector was designed specifically for the single photon search and was optimized to give both a large acceptance for the photons and a high degree of certainty that any additional particles in the event at small angles would be detected. As discussed before, good photon acceptance requires small angle and low energy detection. The ASP detector is constructed from a lead-glass array which can detect photons down to 20° and can veto other particles down to ~ 10°. Lead-glass is well suited to low energy photon detection both because of its good intrinsic resolution, and also because a phototube based system has much less electronic noise than a proportional wire system which allows a clean trigger at *low energies. The full apparatus is shown in Fig.* 13. The central region is the lead-glass array, and the forward detectors are arranged so that scintillators and calorimeters cover the region from 30° to 100 mrad, and 4 planes of drift chambers and a calorimeter cover from 100 mrad to 21 mrad.

ASP – Forward Detectors

The forward region is shown in greater detail in Fig. 14. The lead-glass array provides 5 layers of depth information on the shower deposition of a photon at angles greater than 30 degrees and veto capability down to 10 degrees. Individual elements of the array are offset by $\frac{1}{2}$ elements from layer to layer in order to optimize the resolution of the array along the beam axis and thus to distinguish between real events and beam-gas or beam-halo events. The tungsten mask for

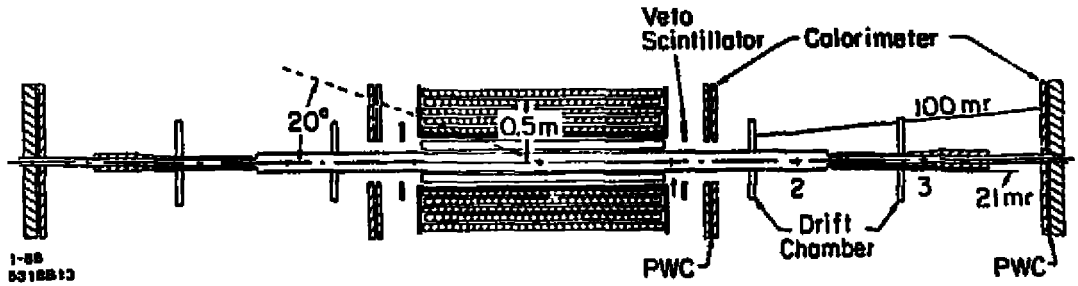

Fig. 13. View along the beam axis of the ASP detector. The apparatus is approximately 8 meters long and 1 meter wide.

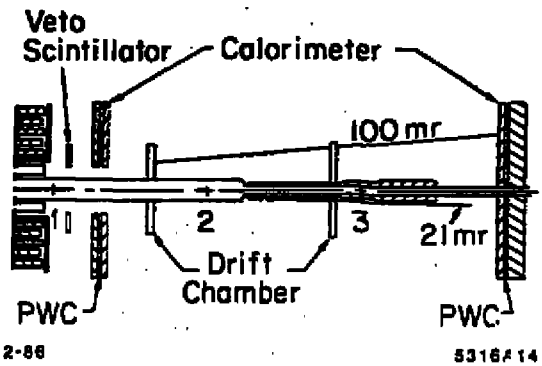

Fig. 14. Forward Detectors.

the apparatus sits in a special indentation in the vacuum chamber. This indentation allows the mask to cover the region between 12 and 20 mrad and thus shield the central array from synchrotron backgrounds. The indentation is also used to minimize the amount of material in front of particles below about 27 mrad. This window can be used to verify that the QED production of $ee\gamma$ events behaves as expected near the kinematic limit for a 0.75 GeV photon transverse momentum. The materials in the vacuum chamber are summarized in Table 1.

Table 1. ASP Vacuum Chamber Materials

Angle (mrad)	Material
> 100	120 mil AL
50 – 100	100 mil AL
45 – 50	Al-stainless weld
30 – 45	stainless flange (3.5 X_0)
27 – 30	60 mil stainless
21 – 27	60 mil stainless @ 30°

Drift chambers are placed in the region in front of the low angle calorimeters in order to measure the exit angles of charged particles in 3 body QED final states. By measuring the angles and energies of forward electron pairs in $ee\gamma$ events, the properties of the photon can be determined by a constrained kinematic fit. The results of such a fit can be used to determine the efficiency for photon reconstruction as well as the resolution for all of the photon parameters. Because angles are in general measured much more precisely than energies, the resolution of the 3-body kinematic fit depends primarily on the angular resolution of the forward drift chambers. The energy resolution of the kinematic fit is small compared to the resolution of the lead-glass array.

Details of the forward calorimeter construction are shown in Fig. 15. A module is constructed from alternating sheets of lead (0.6 cm Pb + 6% Sb), and

Polycast PS-10 acrylic scintillator (1.3 cm). Each $6X_0$ lead-scintillator stack is read out by four sheets of Rohaglas GS1919 wavelength shifter viewed by an Amperex 52212A phototube. The modules are constructed in left and right halves to allow easy assembly around the beam pipe, but care has been taken that there are no gaps in the coverage of the modules. As shown in Fig. 15, this is accomplished by having a 4 cm overlap of the joint in the front and back halves of a module. Two modules are used at 1.5 meters and three are used at 4 meters. The larger number of radiation lengths at small angles is needed to assure that there is no background from QED production of $\gamma\gamma\gamma$ events with non-conversion of the two forward photons. Between modules of each calorimeter are proportional wire chambers used to determine the position of showers in the calorimeter.

The forward shower counter system is a veto and calibration system for the ASP experiment as well as the luminosity monitor for the PEP storage ring. The good forward coverage, small amount of material in front of the calorimeters, and ability to track particles in the small angle region make it an ideal luminosity device. Small angle Bhabha events can also be used to verify the veto performance of the device. Figure 16(a) shows the mean energy of such events as a function of the theta angle with respect to the beam. Coverage extends to angles of about 20 mrad with good uniformity. At approximately 0.12 rad one can see the effect of the transition from showers which are contained in the modules nearest the central calorimeter to those which are contained in the calorimeters at 4 meters. The behavior at .04 rad is due to the presence of a vacuum flange. Figure 16(b) shows the response of the system as a function of the azimuthal angle and illustrates that despite the fact that the modules are constructed in two halves, there is no gap in the coverage. The energy resolution of the forward system is $25\%/\sqrt{E}$ when averaged over the region used as a luminosity region (50 mrad $< \theta <$ 90 mrad). The angular difference between the two electrons in the forward Bhabha events can be used to determine the angular resolution of the system. (See Fig. 17). The total integrated luminosity for the search is determined to be

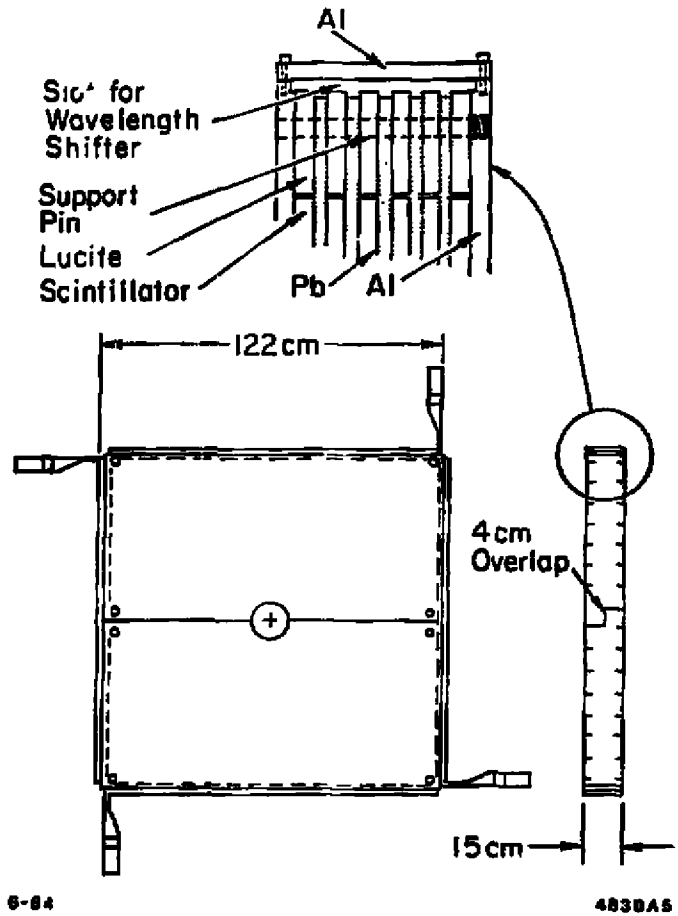

Fig. 15. Forward Shower Counters.

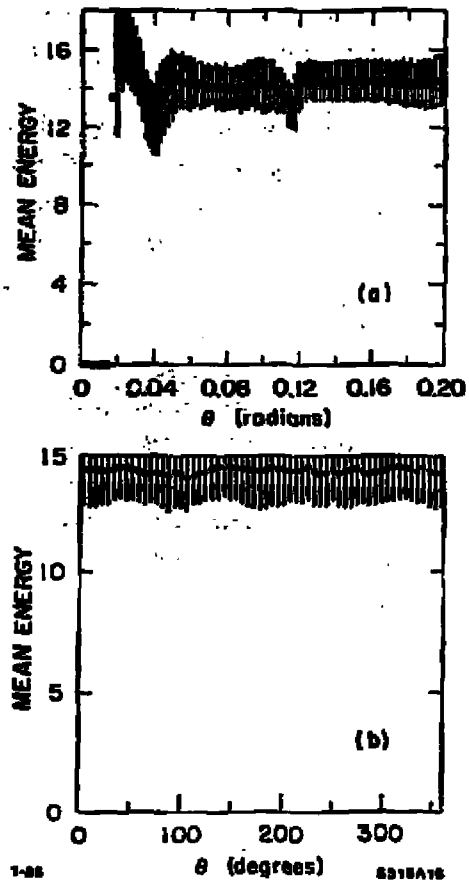

Fig. 16. Mean Energy of Bhabha events in the Forward Calorimeters as a function of (a) θ and (b) ϕ.

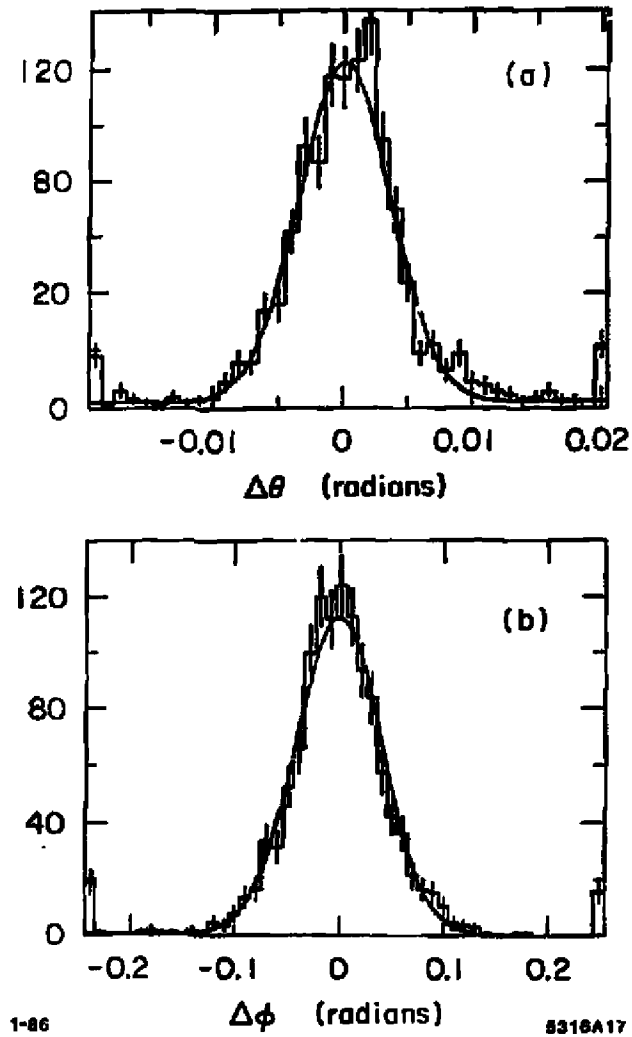

Fig. 17. $\Delta\theta$ and $\Delta\phi$ for Bhabha events in the Forward Calorimeters. $\sigma_\theta = 2.5$ mrad $\sigma_\phi = 28$ mrad.

68.7 pb^{-1}. A comparison of the measured and calculated rates for $\sigma(ee \to ee)$ is shown in Fig. 18.

ASP – Central Detectors

The view of the ASP apparatus along the beam line is shown in Fig. 19. Photons are detected in a five layer deep stack of lead glass bars. Each bar is made from 6 × 6 × 75 cm extruded glass of type F2 (Schott) with 0.35% Ce doping for radiation hardness. Bars are read out at one end by an XP2212PC phototube (Amperex) which is a 12 stage phototube with good noise performance and an attached printed circuit card base. Bars are arranged in a staggered pattern along the beam axis as shown in Fig. 13 to improve the resolution of the stack along the beam axis.

There are 632 bars in the total system arranged in four quadrants of 158 bars each. Each bar has a light fiber which sends light down the axis of the bar to be reflected off the far side and back through the bar to the phototube. This system is used to calibrate and monitor the lead-glass array. All fibers from a quadrant are pulsed by a single Hewlett Packard Superbright LED (HLMP-3950). The LED's are monitored by reference phototubes which also view NaI-Americium pulsers. Individual quadrants are complete subassemblies which can be easily dismounted and transported. The two quadrants on the upper and lower left are mounted together on rails as are the two quadrants on the right. The entire central apparatus can be split apart with a hydrolic drive system to allow easy access to detector elements around the beam pipe and to protect the lead-glass from excess radiation exposure during injection into the storage ring. Each layer of lead-glass is followed by proportional wire chambers constructed from aluminum extrusions. The extrusions are eight-cell closed structures with 1.23 × 2.36 × 200 cm channels with 0.18 cm walls. The wires are 48μ gold-plated tungsten, and 4 extrusions are used to form a PWC plane. The PWC planes provide photon pattern recognition in the xy plane.

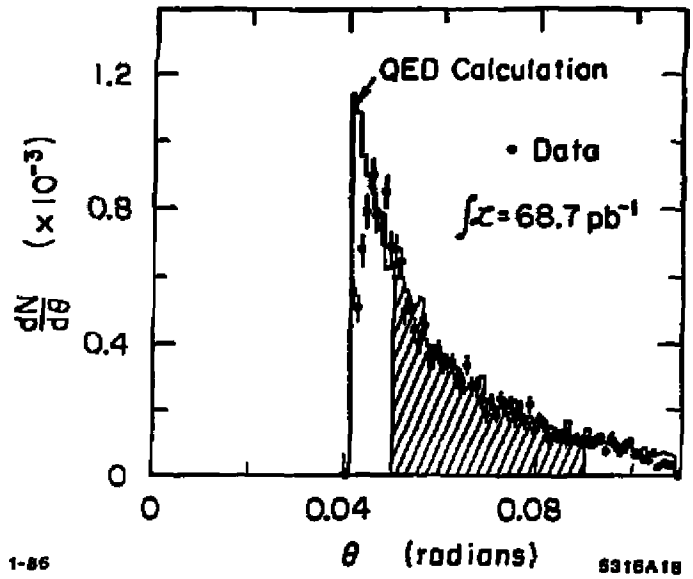

Fig. 18. Data and QED prediction (histogram) for forward Bhabha scattering.

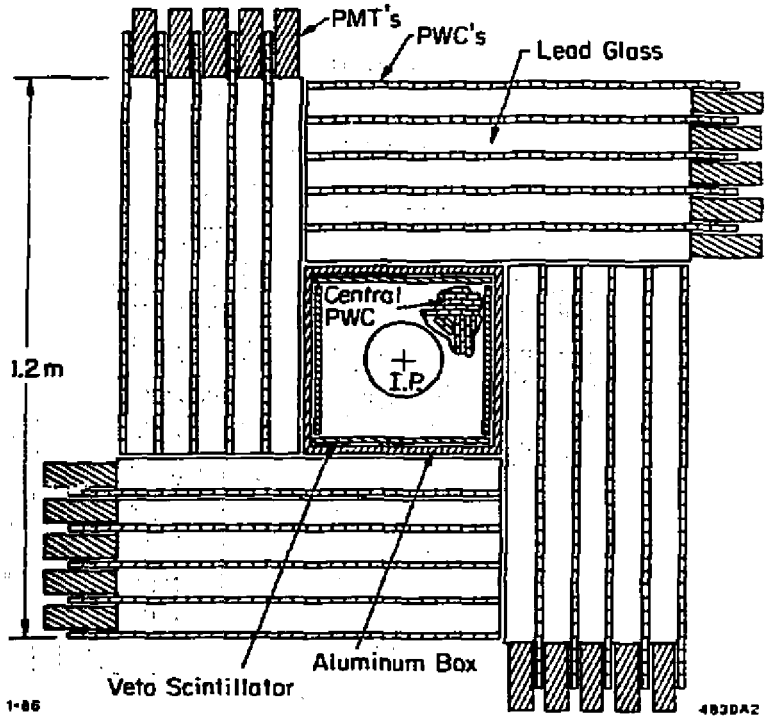

Fig. 19. View along the beam axis of the ASP central detector.

Inside the photon calorimeter are two systems, each of which is designed to adequately reject events with accompanying charged particles and to distinguish between electrons and photons. The innermost system (central tracker, Fig. 20) is made from .9 in × .4 in × 88 in aluminum tubes which are thinned by etching to a wall thickness of .012 in. The wire used is Stablohm 800 and the tubes are read at each end so that the coordinate along the wire can be determined by charge division. The extrusions are glued together to form two L shaped modules which are mounted on a Hexcell backplate and then assembled around the beam pipe. The tubes are arranged so that radial lines from the beam axis do not pass through tube walls, and extra tubes are added at the corners to ensure that charged particles pass through at least five layers. The use of the tube design is intended to ensure that the chamber does not have correlated inefficiencies which would result for example from wires which draw current and the resulting bad field configurations which can occur in open geometries.

Surrounding the central tracker is the second veto system: a 2 cm thick scintillator. Each of the four sides is made from two sheets of 33.5 × 225 × 1 cm Kiowa scintillators. The two sheets could be read separately but at the moment are read by a waveshifter bar and a single phototube. The edges of the scintillators overlap so there are no dead regions.

ASP Trigger

Triggers for the detector consist of two types: monitor triggers and single photon triggers. The single photon triggers are based mainly on analog sums[11] of the pulse heights found in the total lead-glass array, individual quadrants, combinations of layers, or groups of eight bars in a layer. The signals from individual glass bars are sent through passive transformer splitters. One of the signals after the splitter goes to a SHAM-BADC system for the primary readout of the calorimeter. The other signal goes both to the trigger system and a second independent ADC system which is used to verify that missing signals in the

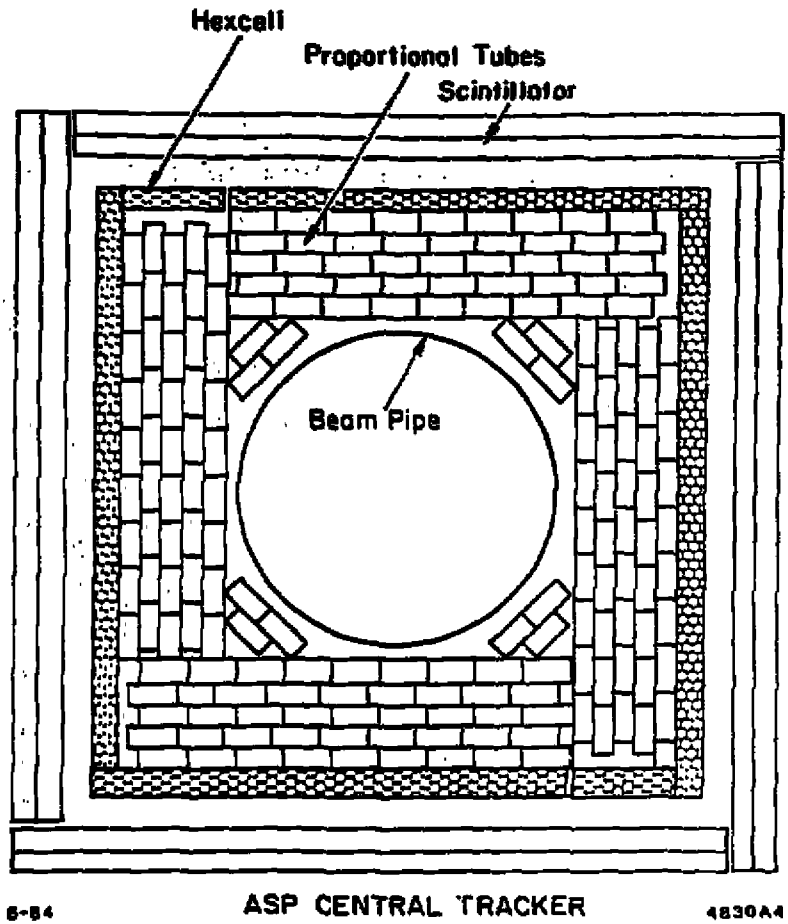

Fig. 20. Central tracker and veto scintillators.

central calorimeter are not the result of electronics failures. (These transformers are also used to break the ground loops between the detector and the summing circuits and produce a lower achievable threshold.) The highest threshold single photon trigger is formed from the analog sum of all 632 bars of lead glass. The threshold for this trigger is however only 1.6 GeV which for photons concentrated around 30° translates to a p_t threshold of 0.8 GeV. The distribution of trigger energies from this trigger on a typical run is shown in Fig. 21(a). The lowest trigger threshold is obtained by requiring fewer than 3 central veto scintillators, $E_{tot} > 0.4$ GeV with at least 0.15 GeV in layers 2 through 5, and energy in the forward system either less than 1 GeV or more than 7 GeV (see Fig. 21(b)). The threshold for this trigger is about 700 MeV or transverse moments of 350 MeV at 30 degrees.

Monitor triggers consist of randoms, cosmics, forward luminosity (Bhabha) triggers and a special trigger for $ee\gamma$ and $\gamma\gamma\gamma$ events. The random triggers are used to determine the level of occupancy in each detector system. These occupancies are in turn used to determine the efficiency of each veto requirement used in the single photon analysis. Typical occupancies are 1% for $E > 40$ MeV in the lead glass and 5% for $E > 100$ MeV in the forward system. Cosmic ray triggers are formed by the coincidence of 2 central veto scintillators in a narrow gate 15 nsec prior to beam crossing. This yields a sample of minimum ionizing tracks roughly in-time with the beam crossing which can be used to monitor the calibration of the lead-glass and also the response of the central system to minimum ionizing tracks. The forward Bhabha triggers are used to determine the luminosity for the search, and finally the $ee\gamma$ triggers are used to provide a sample of single photon events which have all of the same characteristics as signal events except that they have two forward tracks. An example of such an event is shown in Fig. 22.

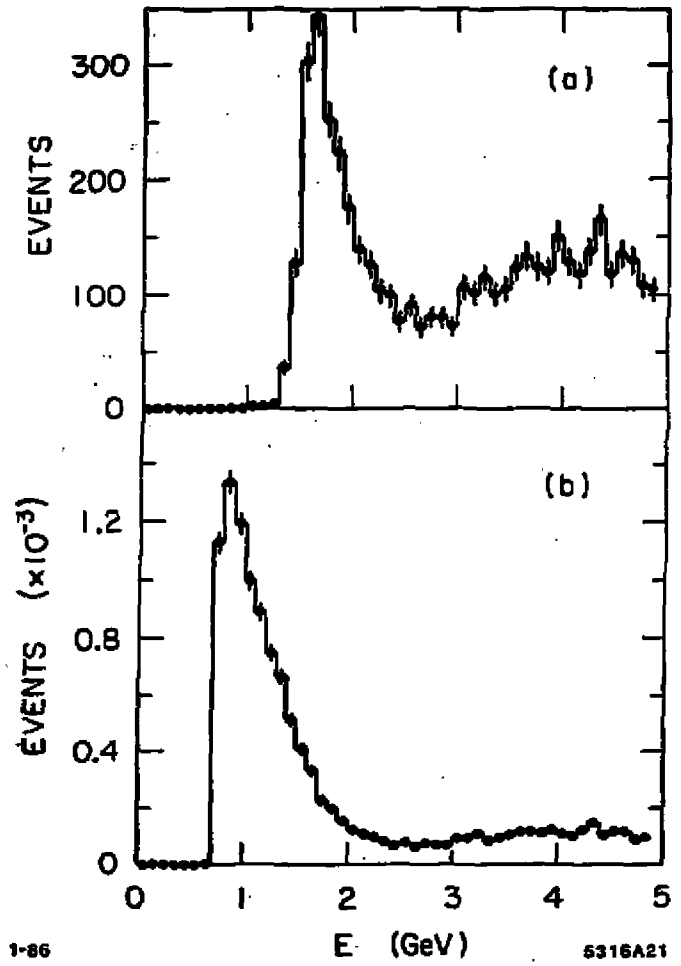

Fig. 21. Number of events versus energy for (a) total energy trigger (b) lowest threshold trigger – *ASP*.

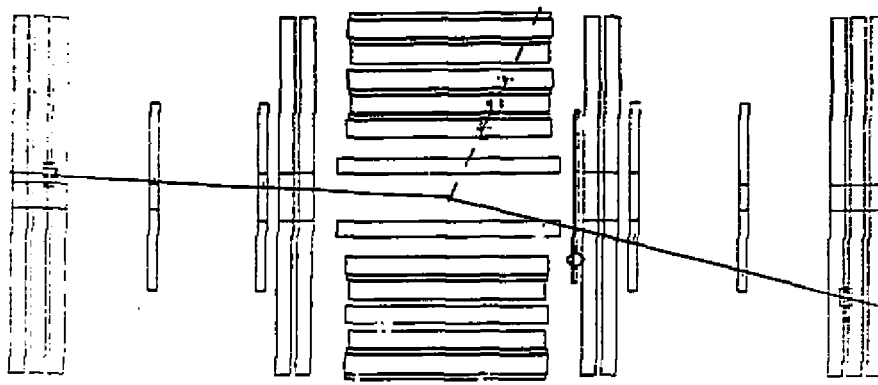

2-86 5316A22

Fig. 22. Typical $ee\gamma$ event used to provide a source of constrained single photons. The vertical scale has been increased by a factor of three.

The $ee\gamma$ Sample

The $ee\gamma$ trigger provides a sample of over 130000 triggers with two forward tracks and an energy deposit greater than 200 MeV in the lead glass. This sample contains both electrons and photons in the central region. By using the measured parameters of all of the tracks in the event, a 4C fit can be done to the hypothesis of a three body final state. Alternatively, using only the measured parameters of the tracks in the forward system, a 1C fit can be done to determine in an unbiased manner the parameters of the track which should be found in the central system. Using this method, the efficiency of the photon pattern recognition algorithm and event cuts as well as the resolution of the photon fitting procedures can be determined. Figure 23 shows the trigger efficiency of the ASP search determined in this way. The efficiency for $p_t^\gamma > 1$ GeV is > 99%. Typical angular resolution in the lead glass is $\sigma_\theta \sim 3.2°$. The energy resolution is $\sim 8\%/\sqrt{E}$ at 60° and $\sim 15\%/\sqrt{E}$ at $20 - 25°$ without correction for energy leakage into the forward calorimeters. The same procedure can be applied to determine the efficiency of all photon pattern recognition cuts. This analysis efficiency is shown in Fig. 24 as a function of the photon energy.

Event Selection

Photon candidates are required to have a cluster of lead-glass bars whose pattern (i.e. which bars are above threshold) is consistent with photon patterns determined from the $ee\gamma$ sample. The time of the lead-glass total energy sum signal (relative to the beam crossing time) as well as the time of each layer of the lead-glass is used to form a time for the event. This time is required to be within $\pm 3\sigma_T$ of the known beam crossing time. The resolution is 2.4 ns at 1 GeV and slightly better at higher energies. Candidate showers are fit to a straight line in the XY plane and the XZ or YZ planes. The projected distance of closest approach to the beam axis in XY is required to be less than 20cm to eliminate cosmic rays, and a value is extracted for R_0, the signed projected distance of

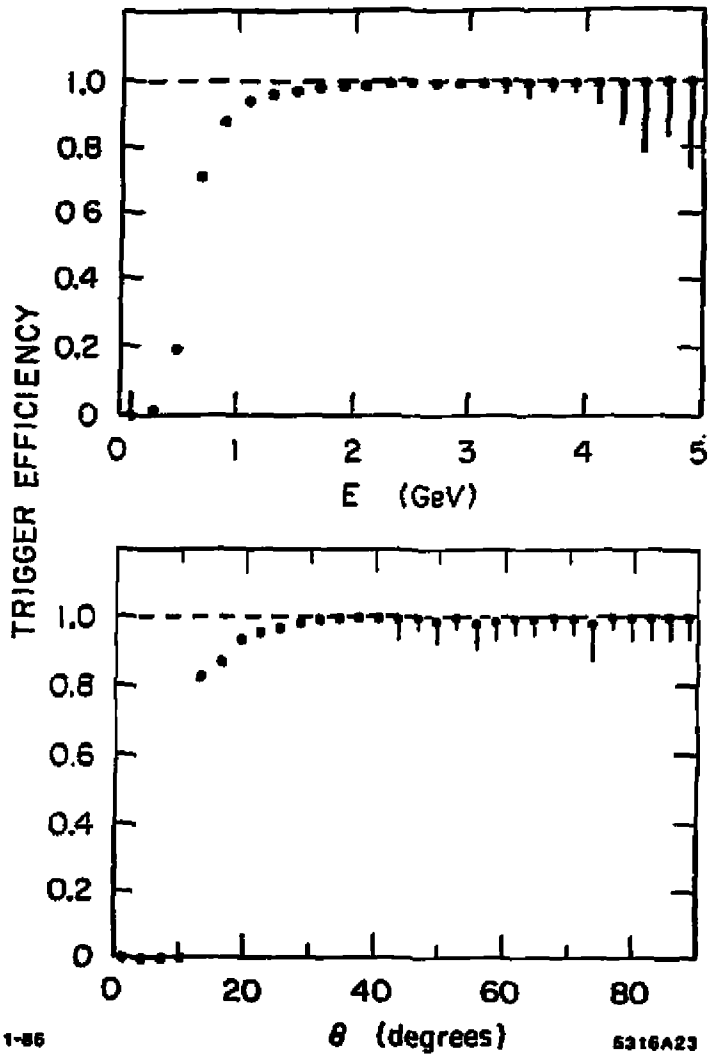

Fig. 23. Trigger efficiency determined using constrained $ee\gamma$ events as a function of (a) Energy and (b) θ. The error bars represent 95% CL limits.

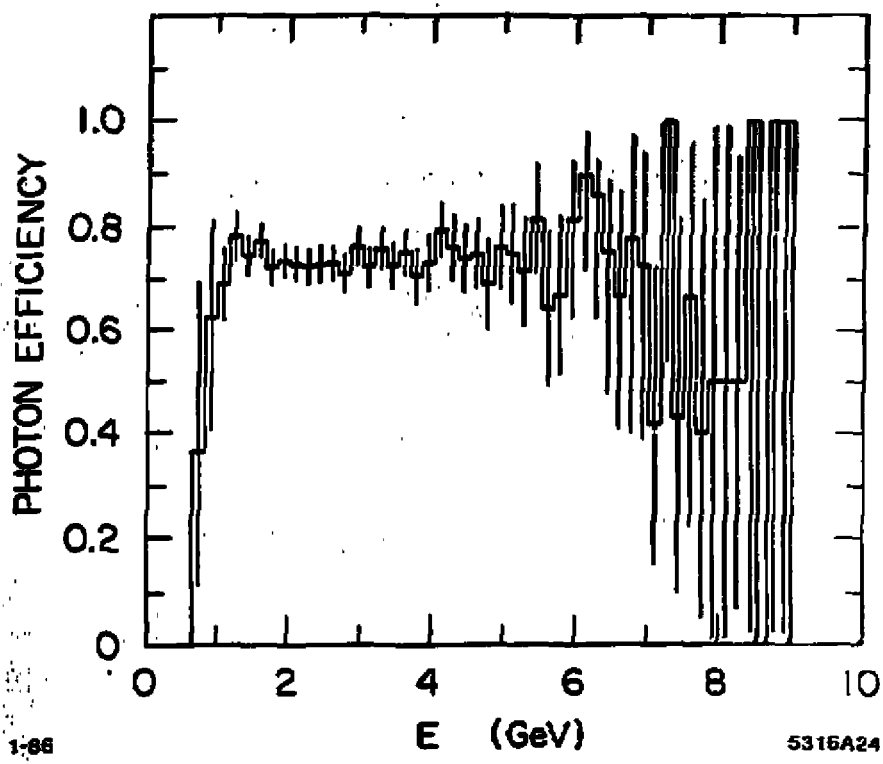

Fig. 24. Efficiency of all cuts applied to the photon candidate versus energy.

closest approach to the beam collision point along the beam axis in the XZ or YZ plane. Photon showers are distinguished from other energy deposits by the loose requirements that the width in each layer be consistent with a photon shower and that the ratio of energy deposited in the front half of the shower to that in the back half be less than 0.5. The average efficiency of all of these cuts is measured to be 75% with little variation in E_γ and θ_γ. The majority of the inefficiency occurs due to reconstruction inefficiency in the pattern recognition software at azimuths where showers span two lead-glass quadrants.

In addition to having a valid photon candidate, an event must have no other charged or neutral particles visible in the detector. The ability to veto against events which do have additional particles depends crucially on the electronic noise levels and occupancies of the components of the detector. Random triggers are used to determine the efficiency for the veto cuts, and $ee\gamma$ events and $\gamma\gamma$ events are used to study occupancies which are correlated to the presence of a photon such as backsplash from the central calorimeter into the central veto scintillators and tracker and leakage into the forward shower modules. The efficiency for all veto cuts is determined to be 60% with the cuts arranged so that no single component of the detector contributes an inefficiency greater than 10%.

The R_0 Distribution

Figure 25 shows the R_0 distribution of events at an early stage of the analysis where there are roughly equal numbers of events coming from QED interactions and beam-gas interactions. Since the latter are to first order uniformly distributed along the beam axis, the R_0 distribution can be used to separate the two contributions. In order to do this, the shape of the distribution for signal and background must be known. The R_0 distribution for signal events is measured with the $ee\gamma$ sample and is shown in Fig. 26(a). The resolution is $\sigma = 3$ cm with a small non-gaussian tail which is approximated by an exponential. The resolution is found to be independent of the transverse momentum of the photon.

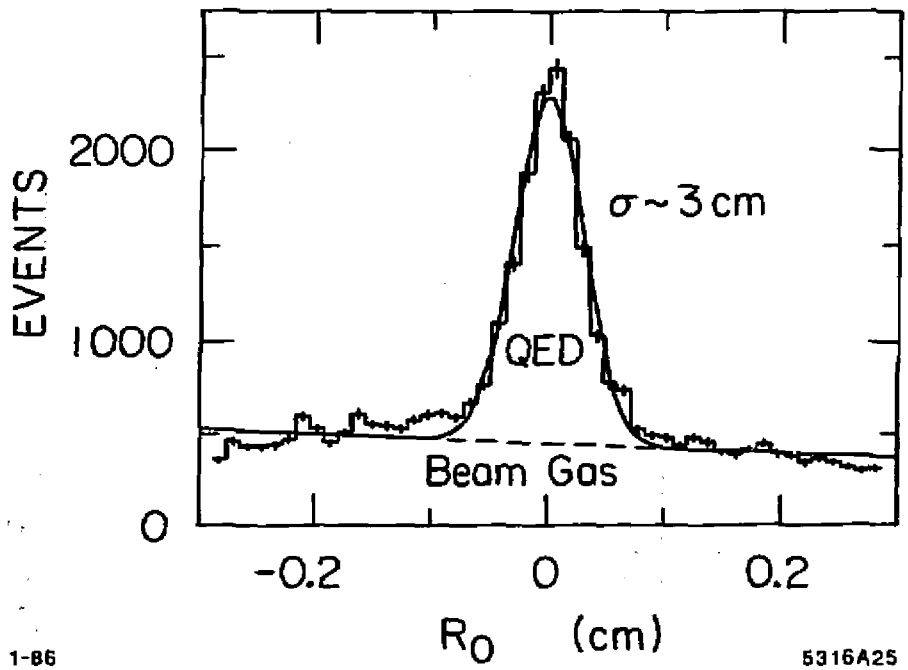

Fig. 25. The R_0 distribution for a mixture of QED and beam-gas interactions.

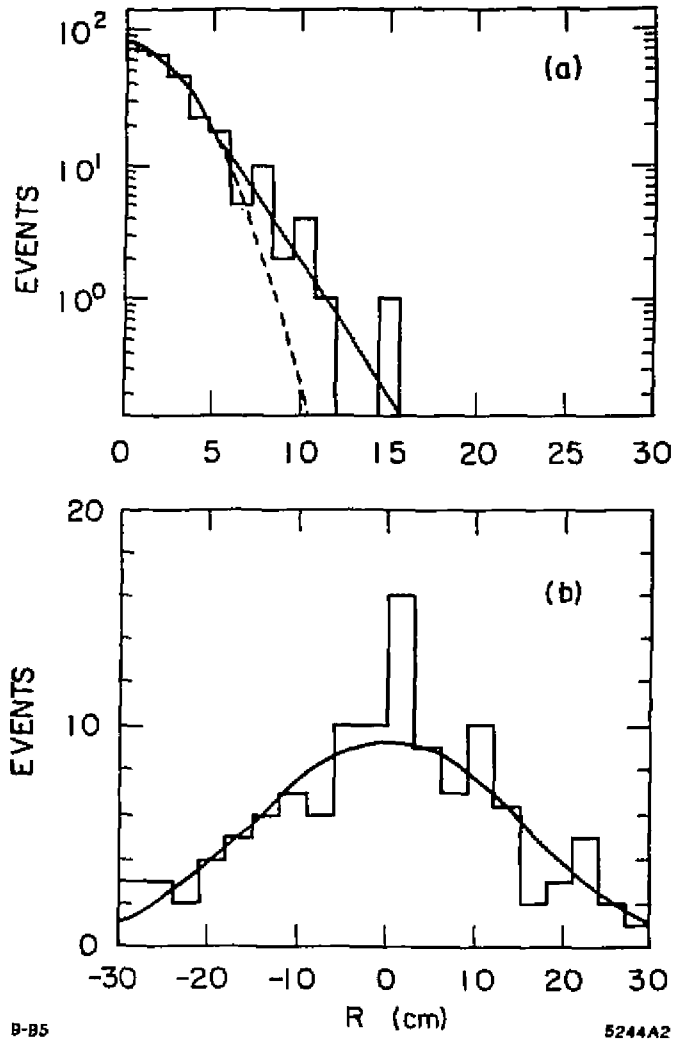

Fig. 26. (a) The R_0 distribution of photons from $ee\gamma$ events. The line is a gaussian with $\sigma = 3$ cm. The non-gaussian contributions are estimated by an exponential tail starting at $R_0 = 6$ cm. (b) The distribution of background events with $p_t^\gamma > 0.6$ GeV/c. The line is a gaussian with $\sigma = 12$ cm.

Electrons have slightly better resolution ($\sigma \sim 2.9$ cm) than photons due to their earlier shower development. The background from beam-gas interactions is observed to be flat in R_0 before the application of several photon pattern cuts that are biased to accept showers from $R_0 < 30$ cm. The shape of the final background is measured by relaxing cuts other than these pattern cuts. (See Fig. 26(b).)

Final Event Sample

Three events with single photon energies consistent with the beam energy were observed in the data sample. These are interpreted as $ee \to \gamma\gamma$ events in which one photon escapes due to non-conversion. A study of observed $\gamma\gamma$ events predicts 1.5 single photons from this source. The requirement $E_\gamma < 12$ GeV determined from an analysis of ee and $\gamma\gamma$ final states eliminates this background with negligible loss of signal acceptance. The final event sample is shown in Fig. 27 for those events with transverse momentum greater than 0.5 GeV/c and polar angle greater than 20 degrees. For the present analysis, we determine a limit using only those events with $p_t^\gamma > 1$ GeV/c. Several methods of using tighter cuts on the identification of candidate energy deposits as photon showers are being studied and should eventually allow the use of the lower energy data to improve the sensitivity of the search.

To obtain the best estimate of the possible number of signal (S) and background (B) events, a maximum-likelihood fit is done to the measured distributions of signal and background events in R_0. For a given true number of signal and background events, the confidence level of this experiment is computed by Monte Carlo as the fraction of equivalent experiments which would estimate a value larger than S. The 90% and 95% confidence level upper limits for the observed distributions are 2.9 and 3.9 events respectively.

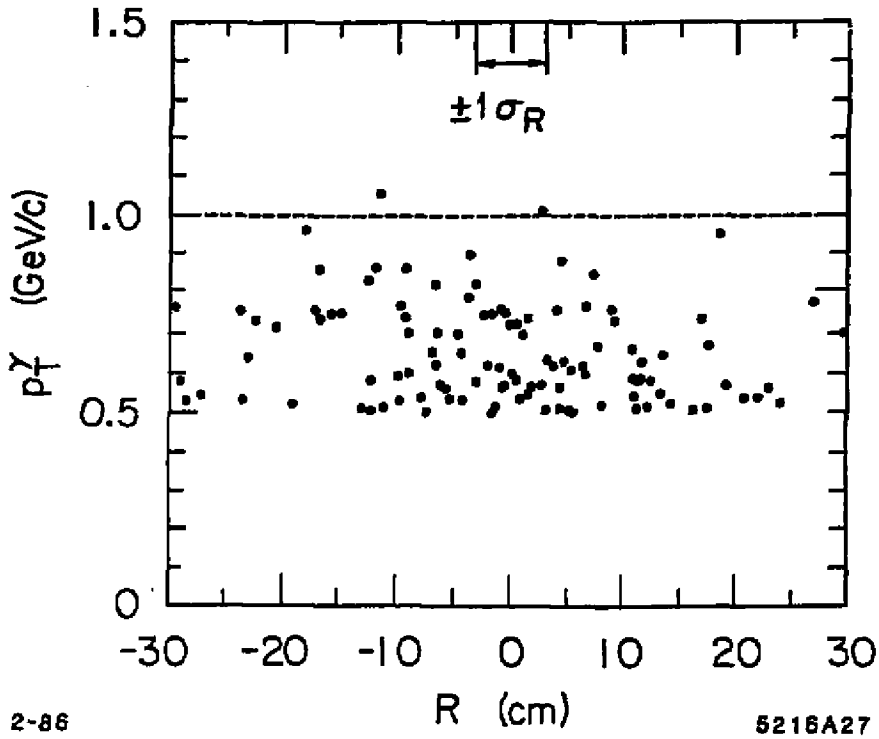

Fig. 27. Final sample of single photon candidates with $p_t^\gamma > 0.5$ GeV/c and $\theta_\gamma > 20°$.

ASP limits

The upper limit of 2.9 events together with the measured luminosity and photon event efficiencies implies that the 90% CL upper limit for the sum of all contributions to the single photon cross-section is

$$\sigma(ee \to \gamma + \text{weakly interacting particles}) < 0.094 \text{ pb}$$

for a photon acceptance defined by $E_\gamma < 12$ GeV, $p_T^\gamma > 1.0$ GeV/c and $\theta_\gamma > 20°$. (Note that this limit is actually more stringent than the MAC limit of 57 fb because the photon acceptance of the ASP apparatus is much larger.) Since the detection efficiency for photons is nearly constant over the signal region in E_γ and θ_γ, the extension of the limit to processes in which the photon energy or angular distribution differs from $\gamma\nu\bar{\nu}$ or $\gamma\tilde{\gamma}\tilde{\gamma}$ is straightforward. The cross-section for radiative pair production of three neutrino generations within the acceptance is 0.032 pb, so the sum of all non-standard model contributions to the cross-section must be less than 0.062 pb

$$\sigma(ee \to \gamma + \text{new sources}) < 0.062 \text{ pb} \quad .$$

Figure 28 shows the dependence of the $\nu\bar{\nu}\gamma$ cross-section on the number of neutrino generations. The limit determined above for the cross-section allows a maximum of 14 generations with 90% confidence. Several features of this limit should be noted. First, unlike many cosmological limits and limits derived from strange meson decays, there is no dependence on the mass of the associated charged lepton partner of the neutrino. Second, the mass of the neutrinos could be of order a few GeV without affecting the limit. The validity of the limit requires no assumption other than the standard model coupling of the Z_0 to a single generation. By contrast, the method of Deshpande et al.[12] extracts N_ν from the ratio of W to Z production in $\bar{p}p$ interactions and requires cancellation of QCD k factors, the branching ratio for both $Z \to \nu\bar{\nu}$ and $W \to e\nu$, and the mass of the top quark.[13]

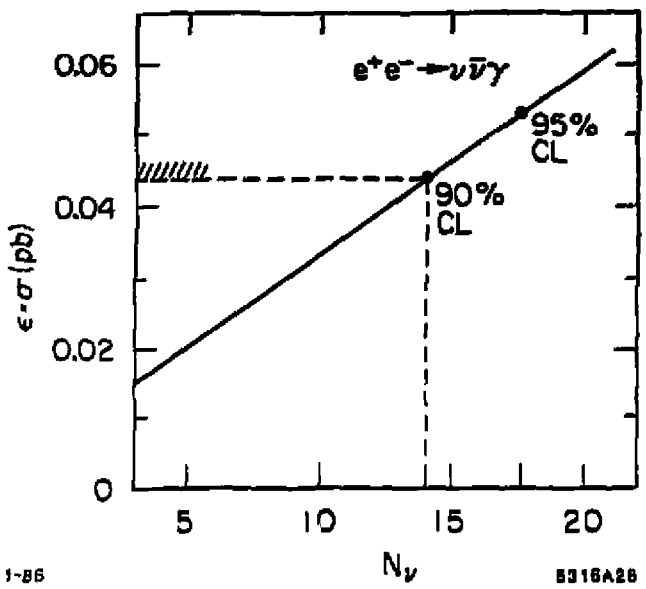

Fig. 28. Corrected $\nu\bar{\nu}\gamma$ cross-section versus the number of neutrino generations.

As can be seen from Fig. 29, all contributions to the γ rate observed at PEP must sum to something slightly less than twice the $\gamma\nu\bar{\nu}$ cross-section. Supersymmetry is the most topical but not necessarily the only source for such additions. In the case of $\gamma\tilde{\gamma}\tilde{\gamma}$ production, the magnitude of the cross-section is determined by the mass of the exchanged virtual selectron (see Fig. 2) and the mass of the final state photinos. The excluded region in these parameters is shown in Fig. 30 both for the case where the left and right handed coupling selectrons ($\tilde{e}_L$, $\tilde{e}_R$) are degenerate in mass and the case where only one contributes to the observed rate. Note that the supersymmetric decay of the Z into pairs of selectrons is excluded for photinos masses up to 6 GeV.

If the lightest supersymmetric particle is the sneutrino (see Fig. 3), then the ASP limit constrains the mass of the wino. From the model of Ref. 6, the 90% CL limit on the mass of the wino is $m_{\tilde{W}} > 48$ GeV/c^2 with the assumptions of massless sneutrinos, no mixing between the wino and higgsinos, and only one light wino ($m_{\tilde{\nu}} = 0$, $O^+ = 1$, and $m_1 \ll m_2$). Other limits can be easily determined by scaling the cross-section to the above assumptions. For the case of light gravitinos, limits on $M_{\tilde{G}}$ can be found using (see Ref. 4)

$$\sigma(\gamma\tilde{\gamma}\tilde{G}) \simeq 2.8 \times 10^{-3}\ \text{pb} \left(\frac{10^{-3}\ \text{eV}}{m_{\tilde{G}}}\right)^2 \frac{s}{(40\ \text{GeV})^2} \ .$$

Finally, if one assumes that at some scale the gauge couplings for strong and electromagnetic interactions become equal and that at that scale the squarks and sleptons are related by $m_{\tilde{q}} = m_{\tilde{l}}$, then the relations between these masses can be calculated at any scale. In particular, at present energies we would have[14]

$$m_{\tilde{q}} \simeq \frac{3}{8} \frac{\alpha_s}{\alpha_{em}} m_{\tilde{e}} \simeq 6.3 m_{\tilde{e}}$$

and

$$m_{\tilde{q}}^2 \simeq 32 m_{\tilde{e}_L}^2 + m_{\tilde{e}}^2 \ .$$

Using these relations, the ASP excluded region can be mapped into the squark,

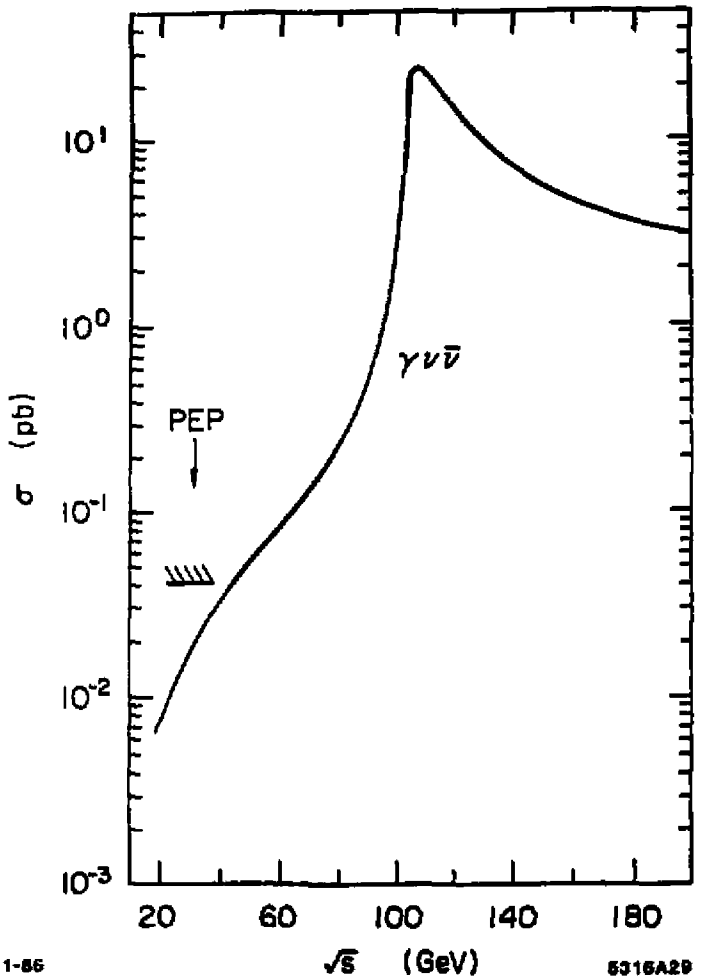

Fig. 29. $\gamma\nu\bar{\nu}$ **cross-section versus** $\sqrt{s}$ **within the ASP acceptance and the ASP limit from PEP.**

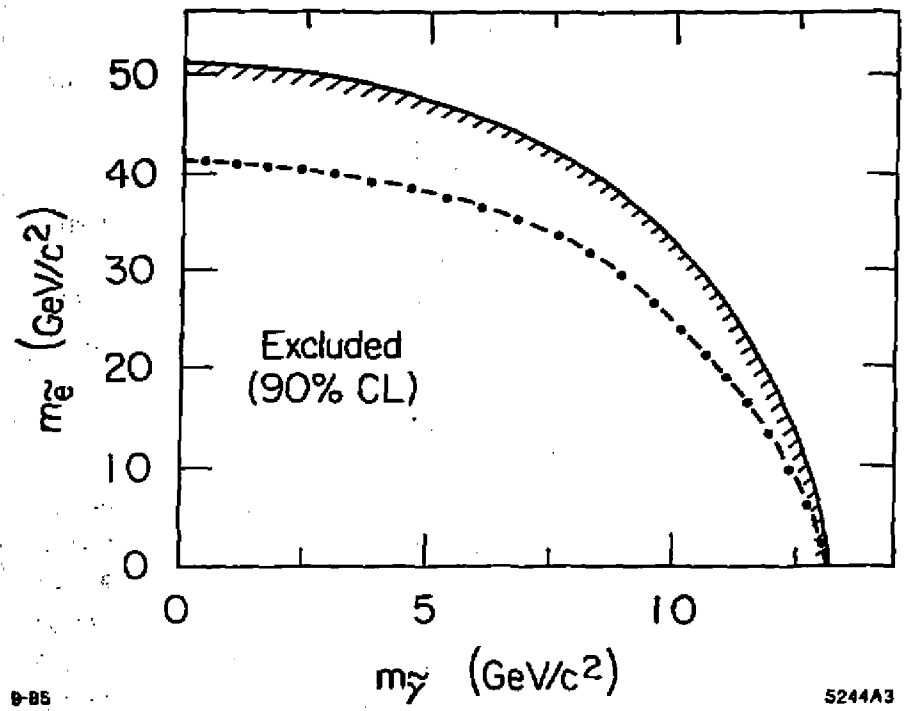

Fig. 30. Region of $m_{\tilde{e}}$ and $m_{\tilde{\gamma}}$ excluded by the present ASP data for $m_{\tilde{e}_L} = m_{\tilde{e}_R}$ (solid curve) and $m_{\tilde{e}_{L,R}} \gg m_{\tilde{e}_{R,L}}$ (dot dashed curve).

gluino mass plane. The excluded region is shown in Fig. 31 together with approximate limits determined from a theoretical analysis of monojet searches[15] and cosmological constraints.[16,17] The cosmological constraint comes from the fact that for every point along the excluded boundary in Fig. 30, the cross-section for massive photino production can be calculated and if the photino is stable, photino production will contribute to the gravitational mass of the universe. For heavy photinos and light selectrons, this contribution can dominate and would violate the observed value of the Hubble constant. In inflationary models of cosmology, the density of the universe is very close to the critical density.[18] In this case, the mass of the photino and selectron can be related by the requirement that the photinos supply the missing dark matter. The allowed values then lie along a line[19] in Fig. 30.

Summary

The technique of detecting a single photon whose transverse momentum can be shown to be unbalanced by any detected particles can provide significant constraints both on our standard model and on important extensions of this model which predict the presence of new particles. The experimental identification of such final states requires that particular care be given both to the acceptance over which the photon can be detected as well as the ability of the detector to observe other particles over a large acceptance with small occupancy. Previous data from the MAC detector and new data from the ASP detector have been presented. The ASP data have reached a sensitivity which excludes any new contributions greater than twice the contribution of $\gamma\nu\bar{\nu}$ events and therefore provide new limits on the number of neutrino generations, the masses of selectrons, photinos, and winos and important restrictions on the masses of squarks and gluinos. Since the method requires only that the photon be accompanied by neutral particles whose interactions are small enough that they do not interact in tens of radiation lengths of material, and since the photon spectrum is rather

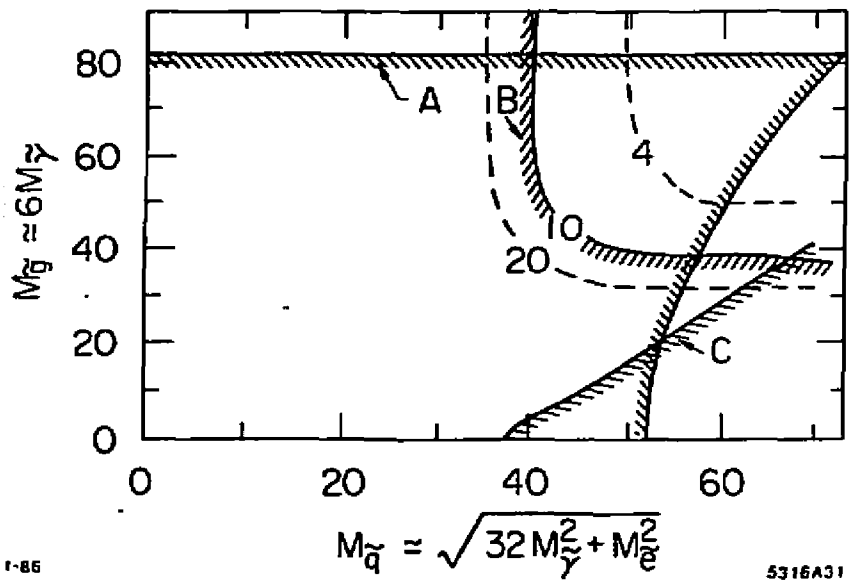

Fig. 31. The excluded region in $m_{\tilde{g}}$ and $m_{\tilde{q}}$ from (A) ASP, (B) monojets (see Ref. 15) and (C) cosmology.

insensitive to the details of the final state, the limit is quite general and can be easily extended to any future models containing particles of this type.

Acknowledgements

I would like to thank J. Ellis, J. Hagelin, P. Fayet, and M. Sher for many useful theoretical discussions, the MAC collaboration for their cooperation in preparing this review and especially the members of the ASP collaboration, for their work on both the apparatus and the data analysis.

REFERENCES

1. E. Ma and J. Okada, Phys. Rev. Lett. 41, 287 (1978); K. Gaemers, R. Gastmans and F. Renard, Phys. Rev. D19, 1605 (1979).
2. S. Wolfram, Phys. Lett. 82B, 65 (1979).
3. See also H. Haber and G. Kane, Phys. Rept. 117, 75 (1985).
4. P. Fayet, Phys. Lett. 117B, 460 (1982).
5. J. Ellis and J. Hagelin, Phys. Lett. 122B, 303 (1983).
6. J.S. Hagelin, G.L. Kane and S. Raby, Nucl. Phys. B241, 638 (1984).
7. J. Ellis, J. Frere, J. Hagelin, G. Kane and S. Petcov, Phys. Lett. 132B, 436 (1983).
8. J. Ellis, Nuffield Workshop, 1982, p. 91.
9. W.T. Ford, in *Proceedings of the International Conference on Instrumentation for Colliding Beam Physics*, edited by W. Ash, 1982, p. 174.
10. E. Fernandez *et al.* (MAC Collaboration), Phys. Rev. Lett. 54, 1118 (1985).
11. R. Wilson, SLAC-PUB-3838, November 1985.
12. N. Deshpande, G. Eilam, V. Barger and F. Halzen, Phys. Rev. Lett. 54, 1757 (1985).
13. See for example L. di Lella, *1985 International Symposium on Lepton and Photon Interactions at High Energies*, Kyoto, Japan.
14. M. Sher, private communication and J. Polchinski, Phys. Rev. D26, 3674 (1982).

15. J. Ellis, *1985 International Symposium on Lepton and Photon Interactions at High Energies*, Kyoto, Japan, CERN-TH-4277/85.

16. H. Goldberg, Phys. Rev. Lett. 50, 1419 (1983).

17. J. Ellis, J. Hagelin, D. Nanopoulos, K. Olive and M. Srednicki, Nucl. Phys. B241, 381 (1984).

18. A. Guth, Phys. Rev. D23, 347 (1981).

19. J. Silk and M. Srednicki, Phys. Rev. Lett. 53, 624 (1984).